

Vortex phase diagram in trapped Bose-Einstein condensation

Takeshi Mizushima, Tomoya Isoshima and Kazushige Machida
Department of Physics, Okayama University, Okayama 700-8530, Japan
(November 6, 2018)

The vortex phase diagram in the external rotation frequency versus temperature is calculated for dilute Bose-Einstein condensed gases. It is determined within the Bogoliubov-Popov theory for a finite temperature where the condensate and non-condensate fractions are treated in an equal footing. The temperature dependences of various thermodynamic instability lines for the vortex nucleation are computed to construct the phase diagram. Experiments are proposed to resolve a recent controversy on the vortex creation problem associated with the quantized vortex observation in ^{87}Rb atom gases.

PACS numbers: 03.75.Fi, 05.30.Jp, 67.40.Vs

I. INTRODUCTION

Since its realization in 1995 [1–3], Bose-Einstein condensation phenomena (BEC) in alkali atom vapors (Na, Li and Rb) have been attracting much attention. Several outstanding fundamental questions such as the relationship between the origin of superfluidity and Bose-Einstein condensation can now address directly both experimentally and theoretically [4,5]. Recently long-sought quantized vortex has been successfully created in ^{87}Rb atom gases by two different experimental methods [6–10]; One is the so-called phase imprinting [6,7] and the other is to use an optical spoon [8–10]. The latter is conceptually similar to the rotating bucket experiment in ^4He and ^3He to create quantized vortices [11]; Here the harmonically trapped BEC with an elongated cigar shape is rotated around the long axis by stirring two laser beams. As the stirred rotation angular frequency Ω increases, a quantized vortex appears at the nucleation frequency Ω_{nuc} , followed by multiple vortices with each carrying the quantized unit circulation. They form an Abrikosov-like lattice structure. The resulting nucleation frequency Ω_{nuc} relative to the radial confining potential ω_{\perp} is $\Omega_{nuc} \sim 0.68\omega_{\perp}$ which is not much dependent on their experimental parameters such as the atom number, or the confining potential, etc. in their experiments [8–10]. This particular number $\Omega_{nuc} \sim 0.68\omega_{\perp}$ sharply disagrees with the prediction [12] by the thermodynamic critical frequency Ω_{global}^L at which the single vortex state becomes stable thermodynamically, namely, a theory based on Thomas-Fermi approximation gives $\Omega_{global}^L/\omega_{\perp} \sim 0.37$. It turns out that the nucleation frequency happens to coincide with the characteristic frequency $\Omega_{w=0}$ at which the non-vortex state ultimately

becomes unstable, leaving only the single vortex state stable globally in the energy configuration space. However, it is argued [13,14] that since the actual nucleation process is more or less related dynamical instability rather than the above thermodynamic quantities, that is, the process is initiated by resonantly exciting the quadrupole mode in a slightly radially distorted cigar-shaped BEC. Thus there is no definite answer to explain Ω_{nuc} at present.

The purpose of the present paper is to complete the vortex phase diagram in the plane; the external rotation frequency Ω versus temperature T in order to help establishing vortex properties in general in the present dilute Bose gas systems, in particular, the nucleation process by identifying the following characteristic critical frequencies related to various thermodynamic instabilities, which will be found to have different T -dependence.

Previously in our series of papers [15–19], we have identified several characteristic critical frequencies; Upon increasing Ω from zero, the single vortex state first becomes locally stable at Ω_{local}^L and then stable globally at Ω_{global}^L relative to the non-vortex state. At further higher frequency $\Omega_{w=0}$ the non-vortex state exhibits an instability toward the vortex state and finally the single vortex state becomes unstable, signalling that multiple vortex state can be stabilized. Here we will investigate the temperature evolution of these critical frequencies by solving the Bogoliubov-de Gennes equation for non-condensates. It is coupled with the generalized Gross-Pitaevskii equation for the condensates within the so-called Popov approximation. The condensate and non-condensates are treated in an equal footing. We assume a cylindrical symmetric system confined radially by a harmonic potential. The rotation occurs around the cylindrical axis.

Stringari [20] gives a phase diagram in the plane; Ω versus T and determines the T -dependence of Ω_{global}^L in our terminology, basing on the Gross-Pitaevskii equation by neglecting the non-condensate contribution. In contrast, we take into account thermally excited non-condensate contribution fully in our calculation as mentioned.

This is one of our continuous efforts to understand the vortex matter in BEC. We have first pointed out the presence of the anomalous negative mode with the particular angular momentum both for the bucket-like system with a rigid wall boundary [15] and for the system with the confining harmonic potential [16]. It turned out later that this anomalous mode in BEC is crucial to understand the vortex matter, in particular, the nucleation problem. Since we find that the non-condensate contri-

bution due to finite temperature effect helps stabilizing the vortex state by pushing up the negative mode, it is of interesting to know the vortex phase diagram in Ω versus T .

The arrangement of the paper is as follows: The formulation of the problem is given within the Hartree-Fock Bogoliubov framework in next section. Based on the self-consistent calculations the local stability of a vortex is considered in III and the global stability is discussed on IV. The final section is devoted to constructing the phase diagram in Ω vs T and discussions.

II. FORMULATION

The Hamiltonian in a rotating frame with the angular frequency with ω is given by

$$\hat{H}_{rot} = \hat{H} - \vec{\omega} \cdot \int \hat{\Psi}^\dagger(\mathbf{r}) \cdot (\mathbf{r} \times \mathbf{p}) \cdot \hat{\Psi}(\mathbf{r}) d\mathbf{r} \quad (1)$$

$$\begin{aligned} \hat{H} = & \int d\mathbf{r} \hat{\Psi}^\dagger(\mathbf{r}) \left\{ -\frac{\hbar^2}{2m} \nabla^2 + V(\mathbf{r}) - \mu \right\} \hat{\Psi}(\mathbf{r}) \\ & + \frac{g}{2} \int d\mathbf{r} \hat{\Psi}^\dagger(\mathbf{r}) \hat{\Psi}^\dagger(\mathbf{r}) \hat{\Psi}(\mathbf{r}) \hat{\Psi}(\mathbf{r}) \end{aligned} \quad (2)$$

where the creation and annihilation operators of the Bose particle are $\hat{\Psi}^\dagger(\mathbf{r})$ and $\hat{\Psi}(\mathbf{r})$. They interact each other with the contact interaction $g \equiv \frac{4\pi\hbar^2 a}{m}$ (a : the scattering length and m : the mass). The confining potential $V(\mathbf{r})$ and μ is the chemical potential. These are decomposed into $\hat{\Psi}(\mathbf{r}) = \phi(\mathbf{r}) + \hat{\psi}(\mathbf{r})$ in terms of the condensate wave function: $\phi(\mathbf{r})$ and the non-condensate part: $\hat{\psi}(\mathbf{r})$. By this decomposition, the above Hamiltonian is rewritten as

$$\begin{aligned} \hat{H}_{rot} = & \int d\mathbf{r} \left[\left\{ \phi^*(\mathbf{r}) h(\mathbf{r}) \phi(\mathbf{r}) + \frac{1}{2} g |\phi(\mathbf{r})|^4 \right\} \right. \\ & + \hat{\psi}^\dagger(\mathbf{r}) \{ h(\mathbf{r}) + g |\phi(\mathbf{r})|^2 \} \phi(\mathbf{r}) + h.c. \\ & + \hat{\psi}^\dagger(\mathbf{r}) \{ h(\mathbf{r}) + 2g |\phi(\mathbf{r})|^2 \} \hat{\psi}(\mathbf{r}) \\ & + \frac{g}{2} \hat{\psi}^\dagger(\mathbf{r}) \hat{\psi}^\dagger(\mathbf{r}) \phi(\mathbf{r}) \phi(\mathbf{r}) + h.c. \\ & + g \hat{\psi}^\dagger(\mathbf{r}) \hat{\psi}(\mathbf{r}) \hat{\psi}(\mathbf{r}) \phi^*(\mathbf{r}) + h.c. \\ & + \frac{g}{2} \hat{\psi}^\dagger(\mathbf{r}) \hat{\psi}^\dagger(\mathbf{r}) \hat{\psi}(\mathbf{r}) \hat{\psi}(\mathbf{r}) \\ & + i\hbar \{ \phi^*(\mathbf{r}) \vec{\omega} \cdot (\mathbf{r} \times \nabla) \phi(\mathbf{r}) \\ & + \hat{\psi}^\dagger(\mathbf{r}) \vec{\omega} \cdot (\mathbf{r} \times \nabla) \phi(\mathbf{r}) \\ & + \phi^*(\mathbf{r}) \vec{\omega} \cdot (\mathbf{r} \times \nabla) \hat{\psi}(\mathbf{r}) \\ & \left. + \hat{\psi}^\dagger(\mathbf{r}) \vec{\omega} \cdot (\mathbf{r} \times \nabla) \hat{\psi}(\mathbf{r}) \right\}]. \end{aligned} \quad (3)$$

The single particle Hamiltonian is

$$h(\mathbf{r}) = -\frac{\hbar^2}{2m} \nabla^2 + V(\mathbf{r}) - \mu. \quad (4)$$

Here we employ the following Bogoliubov-Popov approximation:

$$\begin{aligned} \hat{\psi}^\dagger(\mathbf{r}) \hat{\psi}(\mathbf{r}) \hat{\psi}(\mathbf{r}) & \simeq 2 \langle \hat{\psi}^\dagger(\mathbf{r}) \hat{\psi}(\mathbf{r}) \rangle \hat{\psi}(\mathbf{r}) \\ & + \langle \hat{\psi}(\mathbf{r}) \hat{\psi}(\mathbf{r}) \rangle \hat{\psi}^\dagger(\mathbf{r}) \\ \hat{\psi}^\dagger(\mathbf{r}) \hat{\psi}^\dagger(\mathbf{r}) \hat{\psi}(\mathbf{r}) \hat{\psi}(\mathbf{r}) & \simeq 4 \langle \hat{\psi}^\dagger(\mathbf{r}) \hat{\psi}(\mathbf{r}) \rangle \hat{\psi}^\dagger(\mathbf{r}) \hat{\psi}(\mathbf{r}) \\ & + \langle \hat{\psi}^\dagger(\mathbf{r}) \hat{\psi}^\dagger(\mathbf{r}) \rangle \hat{\psi}(\mathbf{r}) \hat{\psi}(\mathbf{r}) \\ & + \langle \hat{\psi}(\mathbf{r}) \hat{\psi}(\mathbf{r}) \rangle \hat{\psi}^\dagger(\mathbf{r}) \hat{\psi}^\dagger(\mathbf{r}) \\ \hat{\psi}^\dagger(\mathbf{r}) \hat{\psi}(\mathbf{r}) \hat{\psi}(\mathbf{r}) & \simeq 2\rho(\mathbf{r}) \hat{\psi}(\mathbf{r}) \\ \hat{\psi}^\dagger(\mathbf{r}) \hat{\psi}^\dagger(\mathbf{r}) \hat{\psi}(\mathbf{r}) \hat{\psi}(\mathbf{r}) & \simeq 4\rho(\mathbf{r}) \hat{\psi}^\dagger(\mathbf{r}) \hat{\psi}(\mathbf{r}) \end{aligned}$$

with the non-condensate density defined as: $\langle \hat{\psi}^\dagger(\mathbf{r}) \hat{\psi}(\mathbf{r}) \rangle = \rho(\mathbf{r})$. Thus we arrive at the following effective one-body Hamiltonian within the present mean-field approximation:

$$\begin{aligned} \hat{H}_{rot} = & \int d\mathbf{r} \left[\left\{ \phi^*(\mathbf{r}) h(\mathbf{r}) \phi(\mathbf{r}) + \frac{1}{2} g |\phi(\mathbf{r})|^4 \right\} \right. \\ & + \hat{\psi}^\dagger(\mathbf{r}) \{ h(\mathbf{r}) + g |\phi(\mathbf{r})|^2 + 2g\rho(\mathbf{r}) \} \phi(\mathbf{r}) + h.c. \\ & + \hat{\psi}^\dagger(\mathbf{r}) \{ h(\mathbf{r}) + 2g |\phi(\mathbf{r})|^2 + 2g\rho(\mathbf{r}) \} \hat{\psi}(\mathbf{r}) \\ & + \frac{g}{2} \hat{\psi}^\dagger(\mathbf{r}) \hat{\psi}^\dagger(\mathbf{r}) \phi(\mathbf{r}) \phi(\mathbf{r}) + h.c. \\ & + i\hbar \{ \phi^*(\mathbf{r}) \vec{\omega} \cdot (\mathbf{r} \times \nabla) \phi(\mathbf{r}) \\ & + \hat{\psi}^\dagger(\mathbf{r}) \vec{\omega} \cdot (\mathbf{r} \times \nabla) \phi(\mathbf{r}) \\ & + \phi^*(\mathbf{r}) \vec{\omega} \cdot (\mathbf{r} \times \nabla) \hat{\psi}(\mathbf{r}) \\ & \left. + \hat{\psi}^\dagger(\mathbf{r}) \vec{\omega} \cdot (\mathbf{r} \times \nabla) \hat{\psi}(\mathbf{r}) \right\}] \end{aligned} \quad (5)$$

This can be diagonalized by the usual Bogoliubov transformation by noting the commutation relation:

$$\begin{aligned} [\hat{\psi}(\mathbf{r}'), \hat{H}_{rot}] = & \left\{ h(\mathbf{r}) + g |\phi(\mathbf{r})|^2 + 2g\rho(\mathbf{r}) \right. \\ & + i\hbar \vec{\omega} \cdot (\mathbf{r} \times \nabla) \left. \right\} \phi(\mathbf{r}) \\ & + h(\mathbf{r}) \hat{\psi}(\mathbf{r}) + 2g |\phi(\mathbf{r})|^2 \hat{\psi}(\mathbf{r}) \\ & + g \phi^2(\mathbf{r}) \hat{\psi}^\dagger(\mathbf{r}) + 2g\rho(\mathbf{r}) \hat{\psi}(\mathbf{r}) \\ & - i\hbar \vec{\omega} \cdot [\nabla \hat{\psi}(\mathbf{r}) \times \mathbf{r}]. \end{aligned} \quad (6)$$

The Bogoliubov transformation is given by

$$\hat{\psi}(\mathbf{r}) = \sum_{\mathbf{q}} [u_{\mathbf{q}}(\mathbf{r}) \eta_{\mathbf{q}} - v_{\mathbf{q}}^*(\mathbf{r}) \eta_{\mathbf{q}}^\dagger]. \quad (7)$$

The resulting diagonalized form reads

$$\hat{H}_{rot} = E_0 + \sum_{\mathbf{q}} \varepsilon_{\mathbf{q}} \eta_{\mathbf{q}}^\dagger \eta_{\mathbf{q}}. \quad (8)$$

This diagonalization can be accomplished under the following conditions. First we impose the condition on $\phi(\mathbf{r})$ as

$$\{ h(\mathbf{r}) + g |\phi(\mathbf{r})|^2 + 2g\rho(\mathbf{r}) + i\hbar \vec{\omega} \cdot (\mathbf{r} \times \nabla) \} \phi(\mathbf{r}) = 0 \quad (9)$$

which is nothing but the so-called Gross-Pitaevskii (GP) equation containing the non-condensate contribution.

We must fulfill the following equations for diagonalization:

$$\{ h(\mathbf{r}) + 2g|\phi(\mathbf{r})|^2 + 2g\rho(\mathbf{r}) \} u_{\mathbf{q}}(\mathbf{r}) - g\phi^2(\mathbf{r})v_{\mathbf{q}}(\mathbf{r}) - i\hbar\vec{\omega} \cdot \{ \nabla u_{\mathbf{q}}(\mathbf{r}) \times \mathbf{r} \} = \varepsilon_{\mathbf{q}} u_{\mathbf{q}}(\mathbf{r}) \quad (10)$$

$$\{ h(\mathbf{r}) + 2g|\phi(\mathbf{r})|^2 + 2g\rho(\mathbf{r}) \} v_{\mathbf{q}}(\mathbf{r}) - g\phi^{*2}(\mathbf{r})u_{\mathbf{q}}(\mathbf{r}) + i\hbar\vec{\omega} \cdot \{ \nabla v_{\mathbf{q}}(\mathbf{r}) \times \mathbf{r} \} = -\varepsilon_{\mathbf{q}} v_{\mathbf{q}}(\mathbf{r}). \quad (11)$$

This coupled equation is known as Bogoliubov-de Gennes (BdG) equation [21] used both for BEC and for superconductors.

We notice that the eigenfunctions; $u_{\mathbf{q}}(\mathbf{r})$ and $v_{\mathbf{q}}(\mathbf{r})$ satisfy the orthonormalization requirement or the positive norm condition:

$$\int d\mathbf{r} [u_{\mathbf{p}}^*(\mathbf{r})u_{\mathbf{q}}(\mathbf{r}) - v_{\mathbf{p}}^*(\mathbf{r})v_{\mathbf{q}}(\mathbf{r})] = \delta_{\mathbf{p},\mathbf{q}}. \quad (12)$$

The non-condensate density is determined self-consistently by

$$\begin{aligned} \rho(\mathbf{r}) &= \langle \hat{\psi}^\dagger(\mathbf{r})\hat{\psi}(\mathbf{r}) \rangle \\ &= \sum_{\mathbf{q}} [|u_{\mathbf{q}}(\mathbf{r})|^2 f(\varepsilon_{\mathbf{q}}) + |v_{\mathbf{q}}(\mathbf{r})|^2 \{ f(\varepsilon_{\mathbf{q}}) + 1 \}]. \end{aligned} \quad (13)$$

These equations (9), (10) and (11) constitute a complete set of the non-linear coupled equations.

A. Cylindrical system

In order to describe a single vortex threading through the center of the cylindrical symmetric system, it is convenient to use a cylindrical coordinate: $\mathbf{r} = (r, \theta, z)$. We impose the boundary condition that the condensate wave function and the eigenfunctions for the non-condensate vanish at $r = R$, namely, $\phi(r = R) = 0$, $u_{\mathbf{q}}(r = R) = 0$, and $v_{\mathbf{q}}(r = R) = 0$, where R is taken far enough from the center.

The confining potential is given by

$$V(\mathbf{r}) = \frac{1}{2}m(2\pi\nu_r)^2 r^2 \quad (14)$$

and the periodic boundary condition is employed along the z direction. The condensate wave function is written in the form:

$$\phi(r, \theta, z) = \phi(r)e^{i w \theta}. \quad (15)$$

The winding number w is finite when a vortex is present and vanishes when a vortex is absent. In the following we consider the vortex with $w = 1$ only.

The eigenfunctions are also written by the symmetry reasons as

$$u_{\mathbf{q}}(\mathbf{r}) = u_{\mathbf{q}}(r)e^{i q_z z} e^{i(q_\theta + w)\theta} \quad (16)$$

$$v_{\mathbf{q}}(\mathbf{r}) = v_{\mathbf{q}}(r)e^{i q_z z} e^{i(q_\theta - w)\theta}. \quad (17)$$

The eigenvalues $\mathbf{q} = (q_r, q_\theta, q_z)$ may take the following values: $q_r = 1, 2, 3, \dots$, $q_\theta = 0, \pm 1, \pm 2, \dots$, and $q_z =$

$0, \pm 2\pi/L, \pm 4\pi/L, \dots$, where L is the period of the length along the z -axis.

By choosing the external rotation $\vec{\omega} = (0, 0, \omega)$, we obtain the GP equation as

$$\begin{aligned} & \left[-\frac{\hbar^2}{2m} \left\{ \frac{d^2}{dr^2} + \frac{1}{r} \frac{d}{dr} - \frac{w^2}{r^2} \right\} - \mu + V(r) \right. \\ & \left. + g\phi^2(r) + 2g\rho(r) - \hbar\omega w \right] \phi(r) = 0. \end{aligned} \quad (18)$$

Similarly, the BdG equations are now

$$\begin{aligned} & \left[-\frac{\hbar^2}{2m} \left\{ \frac{d^2}{dr^2} + \frac{1}{r} \frac{d}{dr} - \frac{(q_\theta + w)^2}{r^2} - q_z^2 \right\} - \mu + V(r) \right. \\ & \left. + 2g(\phi^2 + \rho) - \hbar\omega(w + q_\theta) \right] u_{\mathbf{q}}(r) \\ & - g\phi^2(r)v_{\mathbf{q}}(r) = \varepsilon_{\mathbf{q}} u_{\mathbf{q}}(r) \end{aligned} \quad (19)$$

$$\begin{aligned} & \left[-\frac{\hbar^2}{2m} \left\{ \frac{d^2}{dr^2} + \frac{1}{r} \frac{d}{dr} - \frac{(q_\theta - w)^2}{r^2} - q_z^2 \right\} - \mu + V(r) \right. \\ & \left. + 2g(\phi^2 + \rho) + \hbar\omega(w - q_\theta) \right] v_{\mathbf{q}}(r) \\ & - g\phi^2(r)u_{\mathbf{q}}(r) = \varepsilon_{\mathbf{q}} v_{\mathbf{q}}(r). \end{aligned} \quad (20)$$

The actual implementation of the numerical computation for these coupled equations is described before [17,18].

B. Free energy

The internal energy E of the system is calculated by taking the Hamiltonian within the mean-field approximation, namely,

$$\begin{aligned} E &= \langle \hat{H}_{rot} \rangle + \mu N \\ &= \int d\mathbf{r} \left[\{ \phi^*(\mathbf{r})h(\mathbf{r})\phi(\mathbf{r}) + \frac{1}{2}g|\phi(\mathbf{r})|^4 \} \right. \\ & \quad + \langle \hat{\psi}^\dagger(\mathbf{r}) \{ h(\mathbf{r}) + g|\phi(\mathbf{r})|^2 + 2g\rho(\mathbf{r}) \} \phi(\mathbf{r}) \rangle + h.c. \\ & \quad + \langle \hat{\psi}^\dagger(\mathbf{r}) \{ h(\mathbf{r}) + 2g|\phi(\mathbf{r})|^2 + 2g\rho(\mathbf{r}) \} \hat{\psi}(\mathbf{r}) \rangle \\ & \quad + \frac{g}{2} \langle \hat{\psi}^\dagger(\mathbf{r})\hat{\psi}^\dagger(\mathbf{r})\phi(\mathbf{r})\phi(\mathbf{r}) \rangle + h.c. \\ & \quad + i\hbar \{ \langle \phi^*(\mathbf{r})\vec{\omega} \cdot (\mathbf{r} \times \nabla)\phi(\mathbf{r}) \rangle + \langle \hat{\psi}^\dagger(\mathbf{r})\vec{\omega} \cdot (\mathbf{r} \times \nabla)\phi(\mathbf{r}) \rangle \\ & \quad + \langle \phi^*(\mathbf{r})\vec{\omega} \cdot (\mathbf{r} \times \nabla)\hat{\psi}(\mathbf{r}) \rangle + \langle \hat{\psi}^\dagger(\mathbf{r})\vec{\omega} \cdot (\mathbf{r} \times \nabla)\hat{\psi}(\mathbf{r}) \rangle \} \\ & \quad \left. + \mu N \right] \end{aligned} \quad (21)$$

or, it can be written as follows:

$$\begin{aligned} E &= \int d\mathbf{r} \left[\{ \phi^*(\mathbf{r})h(\mathbf{r})\phi(\mathbf{r}) + \frac{1}{2}g|\phi(\mathbf{r})|^4 \} \right. \\ & \quad + \langle \hat{\psi}^\dagger(\mathbf{r}) \{ h(\mathbf{r}) + 2g|\phi(\mathbf{r})|^2 + 2g\rho(\mathbf{r}) \} \hat{\psi}(\mathbf{r}) \rangle \\ & \quad + \frac{g}{2} \langle \hat{\psi}^\dagger(\mathbf{r})\hat{\psi}^\dagger(\mathbf{r})\phi(\mathbf{r})\phi(\mathbf{r}) \rangle + h.c. \\ & \quad + i\hbar \{ \phi^*(\mathbf{r})\vec{\omega} \cdot (\mathbf{r} \times \nabla)\phi(\mathbf{r}) \\ & \quad + \langle \hat{\psi}^\dagger(\mathbf{r})\vec{\omega} \cdot (\mathbf{r} \times \nabla)\hat{\psi}(\mathbf{r}) \rangle \} \left. \right] + \mu N \\ &= E_0 + \mu N_0 + \langle \hat{H}_1 \rangle + \mu N_{nc} \end{aligned} \quad (22)$$

where we define

$$E_0 = \int d\mathbf{r} [\phi^*(\mathbf{r})h(\mathbf{r})\phi(\mathbf{r}) + \frac{1}{2}g|\phi(\mathbf{r})|^4 + i\hbar\phi^*(\mathbf{r})\vec{\omega} \cdot (\mathbf{r} \times \nabla)\phi(\mathbf{r})] \quad (23)$$

$$\hat{H}_1 = \int d\mathbf{r} [\hat{\psi}^\dagger(\mathbf{r})\{ h(\mathbf{r}) + 2g|\phi(\mathbf{r})|^2 + 2g\rho(\mathbf{r}) \}\hat{\psi}(\mathbf{r}) + \frac{g}{2}\hat{\psi}^\dagger(\mathbf{r})\hat{\psi}^\dagger(\mathbf{r})\phi(\mathbf{r})\phi(\mathbf{r}) + \frac{g}{2}\hat{\psi}(\mathbf{r})\hat{\psi}(\mathbf{r})\phi^*(\mathbf{r})\phi^*(\mathbf{r}) + i\hbar\hat{\psi}^\dagger(\mathbf{r})\vec{\omega} \cdot (\mathbf{r} \times \nabla)\hat{\psi}(\mathbf{r})]. \quad (24)$$

In terms of the cylindrical coordinate $\mathbf{r} = (r, \theta, z)$, we obtain

$$E_0 = \int dr [\phi^*(r) \{ -\frac{\hbar^2}{2m}\nabla^2 + V(r) - \mu \} \phi(r) + \frac{1}{2}g|\phi(r)|^4 + -\hbar\omega w\phi^2(r)] = \int dr [\phi^*(r) (-\frac{\hbar^2}{2m})\{ \frac{d^2}{dr^2} + \frac{1}{r}\frac{d}{dr} - \frac{w^2}{r^2} \}\phi(r) + V(r)\phi^2(r) - \mu\phi^2(r) + \frac{1}{2}g\phi^4(r) - \hbar\omega w\phi^2(r)]. \quad (25)$$

As shown in Appendix, the total internal energy is now evaluated by the formula:

$$E = \langle \hat{H}_{rot} \rangle + \mu N = 2\pi L \int dr [\phi^*(r) (-\frac{\hbar^2}{2m})\{ \frac{d^2}{dr^2} + \frac{1}{r}\frac{d}{dr} - \frac{w^2}{r^2} \}\phi(r) + V(r)\phi^2(r) + \frac{1}{2}g\phi^4(r) - \hbar\omega w\phi^2(r)] + \sum_{\mathbf{q}} \varepsilon_{\mathbf{q}} f(\varepsilon_{\mathbf{q}}) + \sum_{\mathbf{q}} \varepsilon_{\mathbf{q}} \int d\mathbf{r} |v_{\mathbf{q}}|^2 + \mu \int d\mathbf{r} \rho(\mathbf{r}) \quad (26)$$

where $f(\varepsilon) = 1/\{\exp(\varepsilon_{\mathbf{q}}/k_B T) - 1\}$ is the Bose distribution function.

The entropy S of the system is obtained by the following expression [22]:

$$S = k_B \sum_{\mathbf{q}} \{ \beta \varepsilon_{\mathbf{q}} f(\varepsilon_{\mathbf{q}}) - \ln[1 - \exp(-\varepsilon_{\mathbf{q}}/k_B T)] \}. \quad (27)$$

From eqs. (26) and (27), we can estimate the free energy $F = E - TS$ of the vortex and non-vortex states.

C. Calculated system

In order to perform the self-consistent calculation to determine various characteristic frequencies as a function T , we must specify the parameters: As a typical example, we take up the vortex nucleation experiment on ^{87}Rb atom vapor by Chevy et al [9]. The scattering length $a = 5.5 \times 10^{-9}m$ and atom mass $m = 1.44 \times 10^{-25}kg$ for ^{87}Rb atom. The radial and z axis trapping frequencies are 175Hz and 10.3Hz respectively. We evaluate the density profile of the condensate in Fig.1 by solving the GP equation at $T=0$ for the total number $N = 2.5 \times 10^5$.

The area density along the z axis can be estimated as $n_z = 2 \times 10^9/m \sim 3 \times 10^9/m$ at the center of $r = 0$ as seen from Fig.1(b). In the following the dimensionless ‘‘gas parameter’’ $an_z = 11$ is chosen in the present two-dimensional disk system and the rotation frequency is normalized by the radial confining potential $\omega_{\perp} \equiv 2\pi\nu_r$, denoted by $\Omega \equiv \frac{\omega}{\omega_{\perp}}$ from now on ($\omega_{\perp}/2\pi = 175\text{Hz}$). The system size is set to $R = 7\mu m$ and $L = 5\mu m$. The transition temperature of the present stem $T_{c0} = 207.8nK$ at $\Omega = 0$. The energy is scaled by $\hbar\omega_{\perp} = \hbar\nu_r$.

III. LOCAL STABILITY

A. Local stability of the vortex state

The local stability of the single vortex state is defined by the frequency region bound by the two frequencies: $\Omega_{local}^L < \Omega < \Omega_{local}^U$ where the excitation spectrum is well-defined and no negative frequency exists. We show in Fig.2 the density profiles for the condensate (a) and non-condensate (b) and also the associated excitation spectrum (c) for various Ω values under a fixed T ($T/T_{c0} = 0.4$). As Ω increases, we can see from Fig.2(a) that the condensate is depressed from the outside region while the non-condensate increases its density at the vortex center, filling the vortex core by the non-condensate, eventually a large amount of the non-condensate becomes piling up the outside region for larger Ω values. The filling-in of the non-condensate effectively helps pushing up the so-called anomalous mode, that is, the negative eigenvalue at $q_{\theta} = -1$ toward a positive one as seen from Fig.2(c), resulting in the local stability of the vortex state and giving rise to Ω_{local}^L [23]. In Fig. 2(a) as the inset we display the trace of the negative mode and also the lowest mode at $q_{\theta} > 0$ which becomes negative at Ω_{local}^U at higher Ω 's. It is seen that for $\Omega_{local}^L < \Omega < \Omega_{local}^U$ the excitation spectrum is well defined, implying that a vortex is locally stable in the energy configuration space.

The piling-up of the non-condensate at the outside region arises from the repulsive interaction between the condensate and non-condensate parts. It is rather remarkable to notice from Fig.2(a) in this connection that the vortex core size measured by the peak position of the condensate density is hardly changed under varying Ω .

As T is varied under a fixed Ω , both density profiles of the condensate and non-condensate change into each other shown in Figs.3 (a) and (b) respectively. As seen from Fig.3(a) the core radius defined by the maximum position of the density profile of the condensate slightly increases as T increases. The non-condensate density quickly fills in the central core region and also the outside region as T increases as seen from Fig.3(b). Again the negative eigenmode at $q_{\theta} = -1$ becomes positive at Ω_{local}^L , shown in Fig. 3(b) as the inset. It will be seen

shortly that Ω_{local}^L is a monotonically decreasing function of T .

When we perform the self-consistent calculation, we exclude modes with negative energy in eq.(13). The negative mode(s) represent the instability of system consist of condensate and non-condensate. The steep step in the insets of Fig.2(a) and Fig.3(b) appears when the lowest mode becomes ignored.

B. Local stability of the non-vortex state

The corresponding local stability can be examined for the non-vortex state in a similar way: We show the corresponding example for that case in Fig.4 where (a) and (b) exhibit the density profiles for the condensate and non-condensate respectively. Again as Ω increases, the former (latter) is depleted (piled up) from the outside region. There is no filling-in effect of the non-condensate in this vortex-free state.

The excitation spectrum as depicted in Fig.4(c) shows the appearance of the negative mode at $\Omega_{w=0}$ for certain mode with $q_\theta > 0$. This signals an intrinsic instability of this non-vortex state toward some other state, most likely toward the vortex state in the present situation. The trace of the lowest mode with $q_\theta > 0$ is shown in the inset of Fig.4(a) which is seen to $\Omega_{w=0} = 0.566$ in this case.

The T -dependent properties of this vortex-free state are depicted in Fig. 5: As T increases, the density conversion from the condensate to the non-condensate occurs. This is shown in Figs. 5(a) and (b) where each density distribution is displayed. The inset of Fig.5(a) exhibits the trace of the lowest mode with $q_\theta > 0$, indicating that the negative mode in $q_\theta > 0$ become positive at $T/T_{c0} = 0.4$ in this example.

IV. GLOBAL STABILITY

The relative energies of the non-vortex and the vortex states should change as functions of Ω and T . Lundh et al [12] estimate the energy increment ε per unit length due to the vortex creation for the uniform system at $T = 0$ as

$$\varepsilon = \pi n \frac{\hbar^2}{m} \ln \frac{1.464b}{\xi} \quad (28)$$

where n is the condensate density, b is the radius of a bucket and the coherent length $\xi = 1/8\pi an$. In the presence of the confining potential the above expression is modified to

$$\varepsilon = \pi n_0 \frac{\hbar^2}{m} \ln \frac{0.888R}{\xi_0} \quad (29)$$

with n_0 the peak density, R the trapping radius and $\xi_0 = 1/8\pi an_0$. The angular momentum L per unit length is given by $L = \hbar N$, thus the critical frequency Ω_{global}^L is determined by

$$\varepsilon - \Omega_{global}^L L = 0. \quad (30)$$

Under the Thomas-Fermi approximation this leads to

$$\Omega_{global}^L = 2 \frac{\hbar}{mR^2} \ln \frac{0.888R}{\xi_0} \quad (31)$$

which indicates the global stability of a vortex relative to the non-vortex state, where R is the radius determined by the Thomas-Fermi approximation. At $T=0$ we can easily estimate $\Omega_{global}^L = 0.372$ for the Thomas-Fermi approximation, which is in good agreement with our own calculation $\Omega_{global}^L = 0.382$. Stringari [20] further extends it to finite temperatures by neglecting the non-condensate contribution. We have performed the fully self-consistent calculation, taking into account the non-condensate contribution.

We compare various approximate estimates Ω_{global}^L as a function of T . First the Stringari's Ω_{global}^L is well reproduced by our numerical calculation using the expression (31) where $n_0(T)$ and $R(T)$ are calculated by our self-consistent solution. Starting with eq.(14) and equating the corresponding non-vortex energy, we can evaluate Ω_{global}^L as shown in Fig.6 where curve (2) indicates the result when neglecting the non-condensate contribution while (3) is fully consistent results. It is seen that as T increases two curves deviate progressively showing the importance of the non-condensate contribution. However, curve (3) neglects the effects of the entropy S defined by eq.(27). In fact, the global stability of the vortex state relative to the non-vortex state at finite temperature is defined by the comparison of the two free energies in the system with and without a vortex. The T -dependence of the critical value is plotted as curve (4) in Fig.6.

V. PHASE DIAGRAM AND REMARKS

We show in Fig.7 the four characteristic frequencies; Ω_{local}^L , Ω_{global}^L , $\Omega_{w=0}$ and Ω_{local}^U together with the critical temperature $T_c(\Omega)$. This is estimated as

$$T_c(\Omega) = (1 - \Omega^2)^{\frac{1}{3}} \quad (32)$$

by Stringari [20] for a non-interacting system, which is also approximately valid for the present dilute Bose gas. It is seen that Ω_{local}^L is a decreasing function of T because the non-condensate fraction excited thermally serves as stabilizing a vortex, a fact pointed out already by Isoshima and Machida [16], and also recently by Virtanen et al [23]. $\Omega_{global}^L(T)$ is almost T -independent up to $0.5T_{c0}$ and then quickly increases toward the $T_c(\Omega)$ line. According to eq.(31) they meet tangentially.

As we have discussed on III, the instability of the non-vortex and the single vortex state is defined by the same reason. However, as seen from Fig.7, the critical value of the instability the critical $\Omega_{w=0}$, which correspond to the instability of the non-vortex state, disagrees with the critical Ω_{local}^U . We interpret the disagreement by the following effect. From the eigenvalue equations (19) and (20), we define the effective potential

$$V_{eff}(r) \equiv V(r) + 2g [|\phi(r)|^2 + \rho(r)]. \quad (33)$$

In comparison with the non-vortex state, the density distribution of the condensate $|\phi(r)|^2$ in the vortex state is slightly pushed out because of the angular momentum. As seen from Fig.8(a), this situation is fully understood in terms of $V_{eff}(r)$. As discussed in III, the eigenvalues with $q_\theta > 0$ move down as Ω increases. This means that the non-condensate quickly grows at the edge of the condensate, and the non-vortex state (the single vortex state) becomes unstable at $\Omega_{w=0}$ (Ω_{local}^U). In short, the higher Ω requires in order for the non-condensate to increase at the edge of the condensate in the vortex state, and we find that Ω_{local}^U is always higher than $\Omega_{w=0}$.

The remaining $\Omega_{w=0}$ and Ω_{local}^U are a rather strong increasing function of T . As mentioned before, $\Omega_{w=0}$ turns out to be very near the observed nucleation frequency by Chevy et al [9], which is independent of the details of the experimental parameters used. They find $\Omega_{nuc} \sim 0.68\omega_\perp$. This is compared with our $\Omega_{w=0} = 0.55$, which is nearer than the thermodynamic critical frequency $\Omega_{global}^L \sim 0.39$ at $T = 0$. This may be pure accident, but we can check it by quantitatively examining it through its T dependence.

It is important to notice that $\Omega_{local}^U(T)$ is not much different from $\Omega_{w=0}(T)$ in its value as seen from Fig.7. Thus once a vortex nucleates at $\Omega_{w=0}(T)$, slight increase of Ω brings multiple vortices at $\Omega_{local}^U(T)$, that is, the frequency window of the single vortex state is rather narrow. This is indeed an experimental fact [9] ($\Omega_{nuc}/\omega_\perp = 0.668$, $\Omega_{multi-vortices}/\omega_\perp = 0.697$).

If the system is kept rotating during cooling from above T_c , then the nucleation likely begins when Ω reaches Ω_{local}^L . If the system, cooled already, on the other hand, begins rotating, then at $\Omega_{w=0}$ a vortex may appear. It is known for some time that in superfluid ^4He the former is lower than the latter as expected while in BEC both nucleation protocols give rise to almost same nucleation frequency. This is quite understandable because two frequencies; Ω_{local}^L and $\Omega_{w=0}$ become almost equal at $T = 0$ when the interaction is weak while these two frequencies become quite distinctive when the interaction is strong (see Fig.3 in Isoshima and Machida [18]). It is also true for finite temperatures that the two characteristic frequencies move oppositely upon increasing T as seen from Fig.7. Here there is a good chance to directly confirm the characteristic nucleation frequencies for two different

cooling protocols, a situation quite different from the superfluid ^4He rotating bucket case where the rough surface of a bucket prevents us from knowing the intrinsic nucleation frequency. The present gaseous system is free from this problem.

Quite recently, yet another vortex experiment is reported by Abo-Shaeer et al [24] where many vortices over 100 are observed. The very low nucleation frequency $\Omega_{nuc} \simeq 0.25\omega_\perp$ in their experiment is qualitatively understandable because the gas parameter an_z is large (an order of 500), implying that the characteristic frequencies $\Omega_{w=0}$, Ω_{global}^L and Ω_{local}^L are all small in that region (see again Fig.3 in Isoshima and Machida [18]).

ACKNOWLEDGMENTS

The authors thank K.W. Madison for detailed discussions on their vortex nucleation experiments and also W. F. Vinen for telling us the situation of the vortex nucleation problem in superfluid ^4He .

APPENDIX:

We first express each term of eq. (4) in terms of η^\dagger and η as

$$\begin{aligned} \hat{\psi}^\dagger(\mathbf{r}) \{ h(\mathbf{r}) + 2g|\phi(\mathbf{r})|^2 + 2g\rho(\mathbf{r}) \} \hat{\psi}(\mathbf{r}) &= \sum_{i,j} [\eta_i^\dagger \eta_j \{ u_i^* (h + 2g|\phi|^2 + 2g\rho) u_j \} \\ &\quad + \eta_i \eta_j^\dagger \{ v_i (h + 2g|\phi|^2 + 2g\rho) v_j^* \} \\ &\quad - \eta_i^\dagger \eta_j^\dagger \{ u_i^* (h + 2g|\phi|^2 + 2g\rho) v_j^* \} \\ &\quad - \eta_i \eta_j \{ u_i^* (h + 2g|\phi|^2 + 2g\rho) u_j \}] \\ \hat{\psi}^\dagger(\mathbf{r}) \hat{\psi}^\dagger(\mathbf{r}) &= \sum_{i,j} [\eta_i^\dagger \eta_j^\dagger u_i^* u_j^* + \eta_i \eta_j v_i v_j - 2\eta_i^\dagger \eta_j u_i^* v_j] \\ \hat{\psi}(\mathbf{r}) \hat{\psi}(\mathbf{r}) &= \sum_{i,j} [\eta_i \eta_j u_i u_j + \eta_i^\dagger \eta_j^\dagger v_i^* v_j^* - 2\eta_i \eta_j^\dagger u_i v_j^*] \end{aligned}$$

$$\begin{aligned} i\hbar \{ \hat{\psi}^\dagger(\mathbf{r}) \vec{\omega} \cdot (\mathbf{r} \times \nabla) \hat{\psi}(\mathbf{r}) \} &= i\hbar \sum_{i,j} (u_i^* \eta_i^\dagger - v_i \eta_i) \vec{\omega} \cdot (\mathbf{r} \times \nabla) (u_j \eta_j - v_j^* \eta_j^\dagger) \\ &= -i\hbar \sum_{i,j} (u_i^* \eta_i^\dagger - v_i \eta_i) \vec{\omega} \cdot [\nabla (u_j \eta_j - v_j^* \eta_j^\dagger) \times \mathbf{r}] \\ &= -i\hbar \sum_{i,j} \vec{\omega} \cdot [\eta_i^\dagger \eta_j u_i^* (\nabla u_j \times \mathbf{r}) - \eta_i^\dagger \eta_j^\dagger u_i^* (\nabla v_j^* \times \mathbf{r}) \\ &\quad - \eta_i \eta_j v_i (\nabla u_j \times \mathbf{r}) + \eta_i \eta_j^\dagger v_i (\nabla v_j^* \times \mathbf{r})]. \end{aligned}$$

We substitute these terms into eq.(4) and obtain

$$\begin{aligned}
\hat{H}_1 = & \sum_{i,j} \int d\mathbf{r} [\eta_i^\dagger \eta_j \{ u_i^* (h + 2g|\phi|^2 + 2g\rho) u_j \\
& - \frac{g}{2} u_i^* v_j \phi^2 - \frac{g}{2} u_j v_i^* \phi^{*2} - i\hbar u_i^* \vec{\omega} \cdot (\nabla u_j \times \mathbf{r}) \} \\
& + \eta_i \eta_j^\dagger \{ v_i^* (h + 2g|\phi|^2 + 2g\rho) v_j \\
& - \frac{g}{2} u_j^* v_i \phi^2 - \frac{g}{2} u_i v_j^* \phi^{*2} - i\hbar v_i^* \vec{\omega} \cdot (\nabla v_j \times \mathbf{r}) \} \\
& + (\eta_i \eta_j \text{term}) + (\eta_i^\dagger \eta_j^\dagger \text{term})] \quad (\text{A1})
\end{aligned}$$

where the coefficient of the $\eta_i^\dagger \eta_j$

$$\begin{aligned}
u_i^* (h + 2g|\phi|^2 + 2g\rho) u_j - \frac{g}{2} u_i^* v_j \phi^2 - \frac{g}{2} u_j v_i^* \phi^{*2} \\
- i\hbar u_i^* \vec{\omega} \cdot (\nabla u_j \times \mathbf{r}) \quad (\text{A2})
\end{aligned}$$

is rewritten by using

$$\begin{aligned}
\{ h + 2g|\phi|^2 + 2g\rho \} u_j - g|\phi|^2 v_j \\
- i\hbar \vec{\omega} \cdot (\nabla u_j \times \mathbf{r}) = \varepsilon_j u_j \quad (\text{A3})
\end{aligned}$$

as

$$\begin{aligned}
(8) = \varepsilon_j u_i^* u_j + g\phi^2 u_i^* v_j - \frac{g}{2} u_i^* v_j \phi^2 - \frac{g}{2} u_j v_i^* \phi^{*2} \\
= \varepsilon_j u_i^* u_j. \quad (\text{A4})
\end{aligned}$$

Here we have utilized a relation:

$$\begin{aligned}
\sum_{i,j} \left(-\frac{g}{2} u_i^* v_j \phi^2 - \frac{g}{2} u_j v_i^* \phi^{*2} \right) \\
= \sum_{i,j} \left\{ -\frac{g}{2} u_i(r) v_j(r) \phi^2(r) - \frac{g}{2} u_j(r) v_i^*(r) \phi^{*2}(r) \right\} \\
= \sum_{i,j} (-g\phi^2 u_i^* v_j). \quad (\text{A5})
\end{aligned}$$

Similarly, the coefficient of the term $\eta \eta^\dagger$ in eq.(a7) is found to be

$$-\sum_{i,j} \varepsilon_j v_i^* v_j.$$

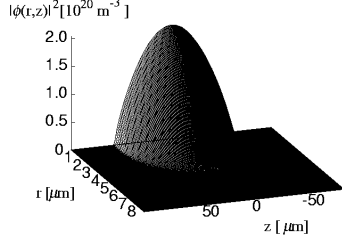
Thus the expectation value of \hat{H}_1 is finally evaluated as follows:

$$\begin{aligned}
\langle \hat{H}_1 \rangle = & \sum_{i,j} \int d\mathbf{r} [\varepsilon_j u_i^* u_j \langle \eta_i^\dagger \eta_j \rangle - \varepsilon_j v_i^* v_j \langle \eta_i \eta_j^\dagger \rangle] \\
= & \sum_i \varepsilon_i \int d\mathbf{r} [|u_i|^2 - |v_i|^2] \langle \eta_i^\dagger \eta_j \rangle - \sum_i \varepsilon_i \int d\mathbf{r} |v_i|^2 \\
= & \sum_i \varepsilon_i \langle \eta_i^\dagger \eta_j \rangle - \sum_i \varepsilon_i \int d\mathbf{r} |v_i|^2 \quad (\text{A6})
\end{aligned}$$

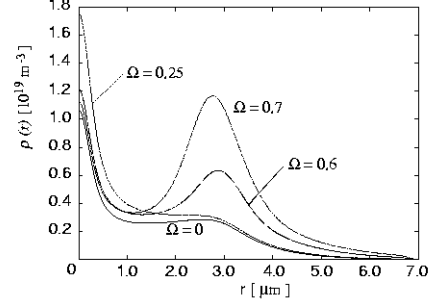
with

$$\begin{aligned}
\mu N_{nc} = & \mu \int d\mathbf{r} \langle \hat{\psi}^\dagger(\mathbf{r}) \hat{\psi}(\mathbf{r}) \rangle \\
= & \mu \int d\mathbf{r} \rho(\mathbf{r}). \quad (\text{A7})
\end{aligned}$$

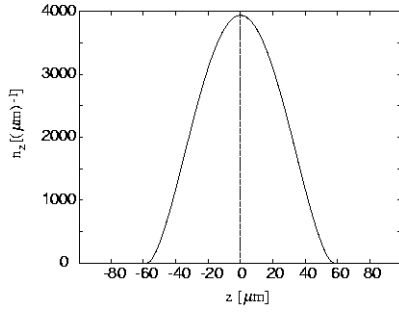
- [1] M. H. Anderson, J. R. Ensher, M. R. Matthews, C. E. Wieman, and E. A. Cornell, *Science* **269**, 198 (1995).
- [2] C. C. Bradley, C. A. Sackett, J. J. Tollett, and R. G. Hulet, *Phys. Rev. Lett.* **75**, 1687 (1995).
- [3] K. B. Davis, M.-O. Mewes, M. R. Andrews, N. J. van Druten, D. D. Durfee, D. M. Kurn, and W. Ketterle, *Phys. Rev. Lett.* **75**, 3969 (1995).
- [4] See for review, F. Dalfovo, S. Giorgini, L. P. Pitaevskii, and S. Stringari, *Rev. Mod. Phys.* **71**, 463 (1999).
- [5] See for review of vortices in BEC, A.L. Fetter, and A.A. Svidzinsky, *cond-mat/0102003*.
- [6] M. R. Matthews, B. P. Anderson, P. C. Haljan, D. S. Hall, C. E. Wieman, and E. A. Cornell, *Phys. Rev. Lett.* **83**, 2498 (1999).
- [7] B. P. Anderson, P. C. Haljan, C. E. Wieman, and E. A. Cornell, *Phys. Rev. Lett.* **85**, 2857 (2000).
- [8] K. W. Madison, F. Chevy, W. Wohlleben, and J. Dalibard, *Phys. Rev. Lett.* **84**, 806 (2000).
- [9] F. Chevy, K. W. Madison, and J. Dalibard, *Phys. Rev. Lett.* **85**, 2223 (2000).
- [10] K. W. Madison, F. Chevy, V. Bretin, and J. Dalibard, *cond-mat/0101051*
- [11] R. J. Donnelly, *Quantized Vortices in Helium II* (Cambridge University Press, Cambridge, U.K., 1991).
- [12] E. Lundh, C. J. Pethick, and H. Smith, *Phys. Rev. A* **55**, 2126 (1997).
- [13] A. Recati, F. Zambelli, and S. Stringari, *Phys. Rev. Lett.* **86**, 377 (2001).
- [14] S. Sinha, and Y. Castin, *cond-mat/0101292*.
- [15] T. Isoshima, and K. Machida, *J. Phys. Soc. Jpn.* **66**, 3502(1997).
- [16] T. Isoshima, and K. Machida, *Phys. Rev. A* **59**, 2203 (1999).
- [17] T. Isoshima, and K. Machida, *J. Phys. Soc. Jpn.* **68**, 487 (1999).
- [18] T. Isoshima, and K. Machida, *Phys. Rev. A* **60**, 3313 (1999).
- [19] T. Isoshima, M. Nakahara, T. Ohmi, and K. Machida, *Phys. Rev. A* **61**, 063610 (2000).
- [20] S. Stringari, *Phys. Rev. Lett.* **82**, 4371 (1999).
- [21] P. G. de Gennes, *Superconductivity of Metals and Alloys* (W.A. Benjamin, New York, 1966).
- [22] S. Giorgini, L. P. Pitaevskii, and S. Stringari, *J. Low Temp. Phys.* **109**, 5040 (1997).
- [23] S. M. M. Virtanen, T. P. Simula, and M. M. Salomaa, *Phys. Rev. Lett.* **86**, 2704 (2001). They claim that the vortex state stays stable, i.e. the lowest mode stays positive even when $\Omega=0$ and also below Ω_{local}^L . This means that thermally stabilized vortex state can exist. However, this vortex state becomes unstable under small perturbations.
- [24] J. R. Abo-Shaeer, C. Raman, J. M. Vogels, and W. Ketterle, preprint.



(a)

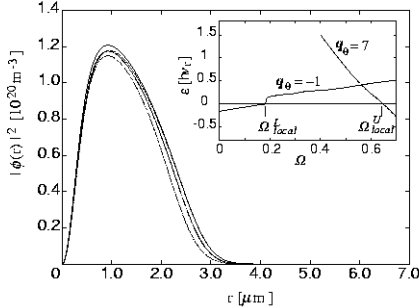


(b)

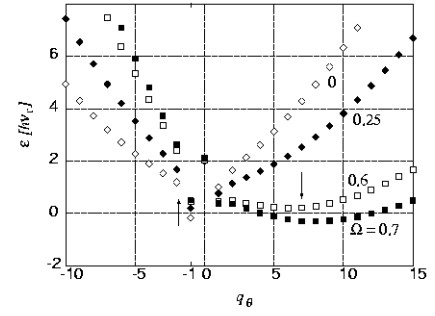


(b)

Fig. 1. The solution of Gross-Pitaevskii equation at $\nu_r = 175Hz$, $\nu_z = 10.3Hz$. (a) Stereographic view of the density distribution of the condensate $|\phi(r)|^2$. (b) The area density n_z per unit length along z -axis at the center $r = 0$. The z -direction of the cylindrical container is assumed to be uniform with the average area density, $n_z = 2.0 \times 10^3/\mu m$ in the following calculation.

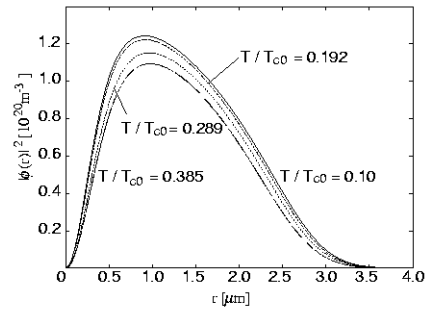


(a)

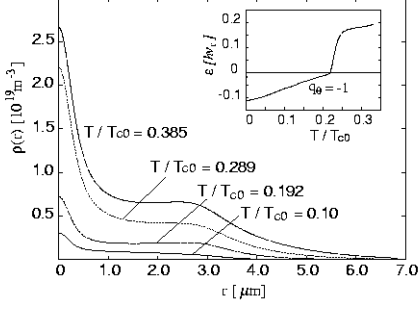


(c)

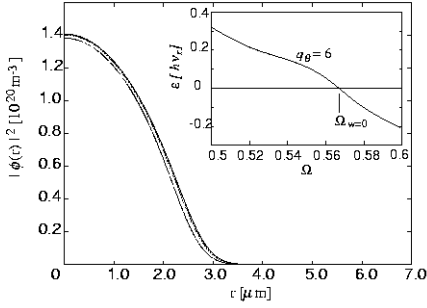
Fig. 2. At $T/T_{c0} = 0.24$, (a) the Ω dependence of the condensate density $|\phi(r)|^2$. The solid, dashed, dotted, dot dashed lines correspond to $\Omega = 0, 0.25, 0.6, 0.7$ respectively. (b) The Ω dependence of the non-condensate density $\rho(r)$. (c) The lowest edge of the eigenvalues along q_θ for $\Omega = 0, 0.25, 0.6, 0.7$. The eigenvalues at $q_\theta = -1$ move up while the eigenvalues in $q_\theta > 0$ move down as Ω increases. The inset in (a) shows the trace of the eigenvalues at $q_\theta = -1$ and $q_\theta = 7$ as a function of Ω .



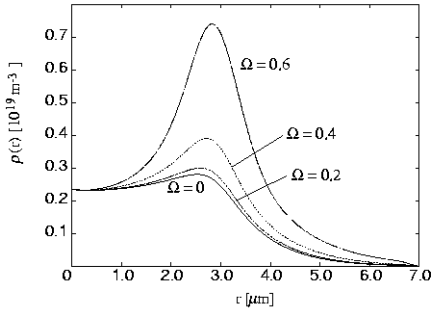
(a)



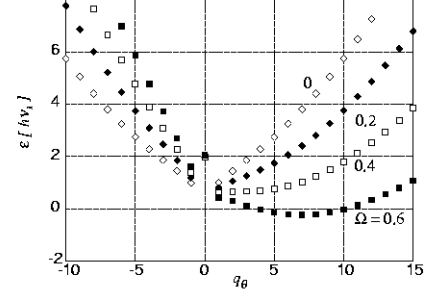
(b)
Fig. 3. At $\Omega = 0.2$, the T -dependence of (a) the condensate density $|\phi(r)|^2$ and (b) the non-condensate density $\rho(r)$. The inset of (b) shows the trace of the eigenvalue at $q_\theta = -1$ as a function of T .



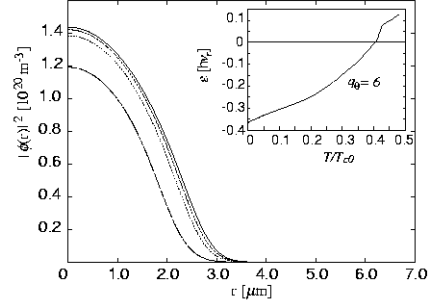
(a)



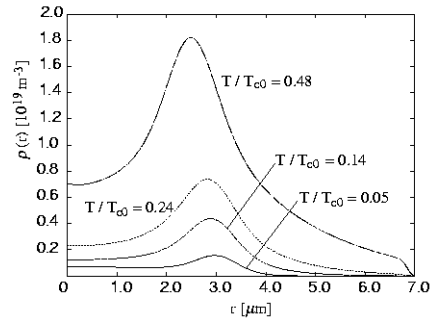
(b)



(c)
Fig. 4. At $T/T_{c0} = 0.10$, the Ω -dependence of (a) the condensate density $|\phi(r)|^2$ and (b) the non-condensate density $\rho(r)$ for the non-vortex state. (c) The lowest edge of the eigenvalues along q_θ for the selected $\Omega = 0, 0.2, 0.4, 0.6$ respectively. The positive eigenvalues in $q_\theta > 0$ become negative as Ω increases. The inset of (a) shows the trace of the eigenvalue at $q_\theta = 6$ as a function of Ω .



(a)



(b)

Fig. 5. At $\Omega = 0.6$, (a) the T -dependence of (a) the condensate density $|\phi(r)|^2$ and (b) the non-condensate density $\rho(r)$ for $T/T_{c0} = 0.05, 0.14, 0.24$ and 0.48 in the

non-vortex state. The inset in (a) shows the trace of the eigenvalue at $q_\theta = 6$ as a function of T .

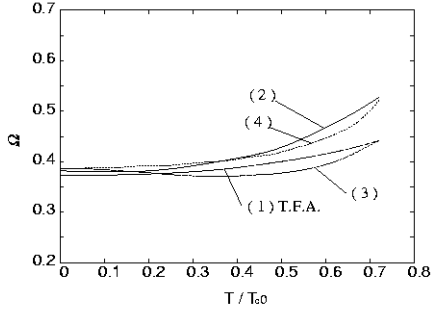
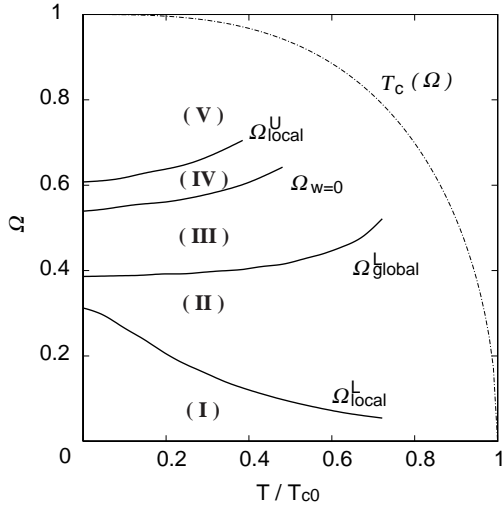


Fig. 6. Curve (1) corresponds to the critical $\Omega_{global}^L(T)$ based on Thomas-Fermi approximation. Curve (2) and (3) express the critical $\Omega_{global}^L(T)$ in which the energy of the vortex state is equal to the non-vortex state under same condition. Curve (2) corresponds to $\Omega_{global}^L(T)$ estimated by neglecting the energy E_0 of the non-condensate while curve (3) corresponds to the critical angular velocity by comparison the total energy E of the vortex and non-vortex state. Curve (4) corresponds to $\Omega_{global}^L(T)$ by comparing the free energies F of the vortex and non-vortex state.

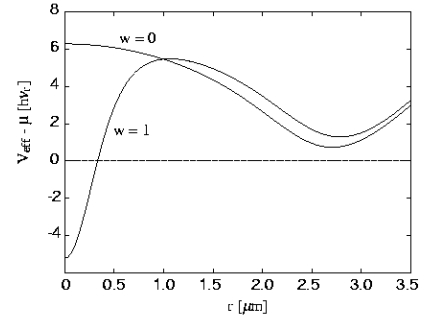


(a)

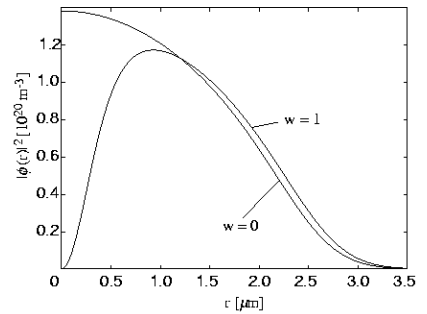
	FREE ENERGY	LOCAL	GLOBAL
(V) ↑ Ω_{local}^U	F ↑ nonvortex vortex	neither	vortex
(IV) ↑ $\Omega_{w=0}$	F ↑ nonvortex vortex	vortex	vortex
(III) ↑ Ω_{global}^L	F ↑ nonvortex vortex	both	vortex
(II) ↑ Ω_{local}^L	F ↑ nonvortex vortex	both	nonvortex
(I) ↑ 0	F ↑ nonvortex vortex	nonvortex	nonvortex

(b)

Fig. 7. Phase diagram: Ω vs T/T_{c0} . (a) the four angular velocities, Ω_{local}^L , Ω_{global}^L , $\Omega_{w=0}$, and Ω_{local}^U together with the critical temperature $T_c(\Omega)$ are plotted as a function of T . These four lines divide the whole area into five regions, (I)-(V). Each of the regions is explained in (b).



(a)



(b)

Fig. 8. At $T/T_{c0} = 0.24$, $\Omega = 0.6$, (a) the effective potential $V_{eff}(r)$ defined by eq.(33) for the vortex state ($w=1$) and the non-vortex state ($w=0$) and (b) the condensate density $|\phi(r)|^2$ in the vortex state and non-vortex state.